MODELLING THE INFLUENCE OF VORTEX SHEDDING ON TRAILING EDGE CUTBACK FILM COOLING AT DIFFERENT BLOWING RATIOS

S. Ravelli - G. Barigozzi

Department of Engineering, University of Bergamo, Dalmine, Italy,
silvia.ravelli@unibg.it, giovanna.barigozzi@unibg.it

ABSTRACT

This numerical investigation deals with the capability of unsteady modelling to predict the mixing between the mainstream and the coolant exiting the trailing edge cutback slots in a high pressure turbine nozzle guide vane. The trailing edge cooling features a pressure side cutback with 8 film cooling slots, stiffened by evenly spaced ribs in an inline configuration. Several values of the coolant-to-mainstream mass flow ratio were considered, i.e. *MFR* = 1.05%, 1.44% and 2%, under incompressible-flow assumption.

With a focus on the cases at medium and high *MFR*, results from the Scale-Adaptive Simulation (SAS) and Detached Eddy Simulation (DES) were compared with experimental measurements including not only cooling effectiveness distributions over the cutback surface but also data from PIV and flow visualizations, with the aim of documenting the inherent instability of the coolant/mainstream flow downstream of the cutback lip. Vortex shedding and cooling effectiveness in the cutback region were reasonably predicted by SAS and DES. However, the simulated thermal coverage at the trailing edge was overestimated for the highest *MFR*.

NOMENCLATURE

$BR = U_{c,slot} / U_{e,x/L=0} * \rho_c / \rho_\infty$	blowing ratio
c	vane chord
CFL	Courant-Friedrichs-Lewy
D	hole diameter
f	frequency
H	vane height
L	rib length
L_c	cutback length
M	Mach number
$MFR = m_c / m_\infty$	coolant-to-mainstream mass flow ratio
$MFR_{slot} = m_{c,slot} / m_\infty$	
$\mathrm{Re}_{2,is} = U_{2,is} c / \nu$	isentropic outlet Reynolds number
s	vane pitch, slot height
$St = tf / (0.5(U_{e,x/L=0} + U_c))$	Strouhal number
t	lip thickness
T	temperature
U	velocity
$VR = U_{c,slot} / U_{e,x/L=0}$	velocity ratio
X, Y, Z	axial, tangential, spanwise direction
w	slot width
ν	kinematic viscosity
$\eta = (T_{aw} - T_\infty)/(T_c - T_\infty)$	adiabatic effectiveness
$\theta = (T_{gas} - T_\infty)/(T_{c,out} - T_\infty)$	normalized temperature
ω	spanwise vorticity

Subscripts

1	inlet
2	exit
av	lateral average
aw	adiabatic wall
ax	axial
c	coolant
e	free stream
is	isentropic condition
out	at the hole exit
slot	computed at the slot exit
t	turbulent
∞	mainstream

INTRODUCTION

This paper represents a continuation of previous studies by the same authors on the modeling of trailing edge cutback film cooling in a high pressure turbine nozzle guide vane, at different *MFR* values, i.e. *MFR* = 1.05%, 1.44% and 2%. The main aim is to simulate the adiabatic effectiveness levels measured over the cutback surface in lab tests at EST (Energy Systems and Turbomachinery Laboratory of Bergamo University). It turned out a challenging goal. Whatever the *MFR*, the steady Reynolds-averaged Navier–Stokes (RANS) approach was found to overpredict the cooling effectiveness on the cutback surface (Ravelli and Barigozzi (2013)). The overestimation of the cooling effectiveness resulted more and more significant with increasing distance from the cutback slot exit. Since discrepancy between RANS predictions and measured thermal coverage at the trailing edge was attributable to the unsteadiness that exists behind the cutback lip, unsteady modeling was implemented to evaluate improvements in simulating the mixing between the mainstream and the coolant exiting the cutback slot. In order of increasing complexity, Unsteady RANS (URANS) simulations were run first. As shown in Ravelli and Barigozzi (2014), URANS was a little better than RANS at predicting the deterioration of film cooling effectiveness along the cutback surface only at the lowest *MFR* of 1.05%, but agreement with the measured η was still far from being achieved. It was necessary to run SAS to get a reasonable pattern of adiabatic effectiveness, showing a poor thermal protection (η < 0.2) at the trailing edge, as observed experimentally. SAS was proven to be suitable for modeling trailing edge cutback film cooling at *MFR* of 1.05%.

In the present study SAS and DES are tested at higher *MFR* values (1.44% and 2%). A change in the flow rate of coolant discharged through the cutback slot affects the *VR*, which ultimately determines the vortex shedding in the cutback region. When the *VR* is near one, the mainstream-side and the coolant-side vortices have similar strength whereas, at *VR* > 1, the flow behind the lip is dominated by the counter clockwise coolant-side vortices. Note also that running unsteady simulations is critical when it comes to increasing *VR* as unsteadiness may be dampened out, thus resulting in steady-like flow. URANS could not prevent this from happening at *VR* > 1, this is why advanced eddy simulations are used here.

In the technical literature, SAS or DES models have been successfully applied to trailing edge film cooling on simplified cutback geometry. Joo and Durbin (2009) invoked the SAS method for *BR* = 1 and 1.5. They demonstrated that eddy simulations can produce a close agreement to measured film effectiveness data on the cutback, with no need for artificial forcing. The potentials of SAS for industrial flow simulations, including trailing edge cutback film cooling, were highlighted by Egorov et al. (2010). They applied the Shear Stress Transport SST-SAS to a simplified blade geometry as reported in Martini et al (2003). The predicted values of the spanwise averaged film cooling effectiveness were close to those measured on the cutback. Martini et al. (2005) applied DES to three different cutback models, for three blowing ratios (*BR*= 0.50, 0.80 and 1.10): time averaged film cooling effectiveness showed very good agreement with experimental data. DES instantaneous results revealed that vortical structures carry the hot fluid to the cutback surface, diminishing the thermal coverage at the trailing edge. DES was also chosen by Krueckels et al. (2009) to design an optimized geometry of pressure side bleed trailing edge cooling. Accuracy in DES predictions of laterally averaged film cooling effectiveness on the cutback was verified against measurements in a low speed test rig. Schneider et al. (2010 and 2012) reported on Large Eddy Simulations (LES) of Martini's trailing edge model, without land extensions and internal cooling design. They assessed that changing either the blowing ratio or the flow regime of the coolant can affect the large coherent structures which are periodically shed at the cutback lip and, consequently, the mixing process. Statistical flow field quantities and film cooling effectiveness matched reasonably the experimental data. However no measurements were available for comparison with the instantaneous snapshots of LES showing temperature and velocity fluctuations contours in the cutback region, for different blowing ratios in the range between 0.35 and 1.4.

It follows that the Scale-Resolving Simulation (SRS) approach is required for correctly predicting vortex shedding from the cutback lip but no clear indication of the most effective method to use (among SAS, DES or LES) can be inferred from references. Hence the scope of the present work is to provide a kind of application guideline for SAS and DES, when trailing edge cutback film cooling is modeled in a realistic nozzle guide vane cascade, at high blowing ratios. The main goal is to get predictions of cutback thermal coverage as close as possible to measurements, while minimizing the computational cost of the SRS. In particular the cases at MFR = 1.44% and 2% are taken into account so that experimental data available in Barigozzi et al. (2012) can be used for validation purposes. The available measurements include PIV data and flow visualizations on the cutback mid-plane.

COMPUTATIONAL SETUP

All simulations were performed using commercial software Fluent v14.5. Both SAS and DES ran on 64 (2.10 GHz) processors of a LINUX cluster. Grids were generated using Pointwise software by Pointwise, Inc. Geometry of the cooled vane, 3D computational domain and final grid are the same as those used in Ravelli and Barigozzi (2014).

Vane geometry and 3D domain

Different views of the cooled vane are shown in Fig. 1. A profile typical of current first-stage nozzle guide vane design in heavy duty gas turbine has been taken into account: it is characterized by a pitch to chord ratio of 1.04 and an aspect ratio of 0.69. The flow turning angle at design point is 73.5°. The cooling scheme includes two staggered rows of cylindrical holes and a trailing edge cutback, all located on the pressure side. Cooling air from the cavity is partly ejected through the cooling holes and partly fed through the cutback slots to achieve trailing edge protection. The first (X/c_{ax} = 0.52) and the second row (X/c_{ax} = 0.64) of holes are composed of 23 and 24 cooling holes, respectively. The diameter of the cooling holes D is 1.05 mm. Within each row, the hole-to-hole pitch is 2.76D and the hole length is 4.9D. The holes are angled at 30° to the surface. Holes and cutback are spread over 70% of the vane height. The cutback (X/c_{ax} = 0.72) consists of eight equally spaced rectangular slots 6.75 × 1.43 mm in size, corresponding to a slot width to height ratio w/s of about 4.7. A rounded ejection lip profile (1.4 mm thick) was utilized resulting in a lip thickness to slot height ratio t/s of about 1.0. In order to increase the stiffness of the thin trailing edge and to enhance the internal heat transfer, a rib array was adopted (Fig. 1). The coolant enters the plenum along the spanwise direction then it is channeled in between the ribs. Afterwards, it is discharged through the cooling holes and finally through the cutback slots.

With the aim of reducing the computation effort, simulations were run on only one cutback slot. Symmetry planes at the mid-planes of the 1st row - jet were set to simulate a section of the vane passage including two cutback slots (i.e. the vane central slots, see the dashed rectangle in Fig. 1). The second symmetry condition is at the lateral faces of the domain, as shown in Fig. 2. This computational domain setting was based on the assumption that the coolant cavity in the real airfoil is uniformly filled so that the central slots are fed quite homogeneously from opposite sides. That has already been proven to capture the physics of the coolant exiting the plenum to the external pressure side of the vane, at least when steady modeling is performed (Ravelli et al. (2013)).

The 3D domain consisted of the upstream plenum, the coolant channels, the trailing edge cutback and the vane passage. Periodicity conditions in the tangential direction were applied to simulate multiple vane passages in a linear arrangement. The inlet of the passage was located 1.6 c_{ax} upstream of the vane leading edge, where mainstream velocity and turbulence measurements were available from experiments. The outlet was located well downstream. The boundary conditions prescribed constant velocity inlet for the mainstream (20.7 m/s) and static pressure at the outlet (97200 Pa), in order to assure M_{2is} of 0.2 (Re_{2is} = 6.5 10^5). The mainstream turbulence intensity and length scale were 1.62% and 10.4 mm, respectively. Both mainstream and coolant flow were assumed to be air whose temperature was set at T_∞ = 298 K and T_c = 323 K.

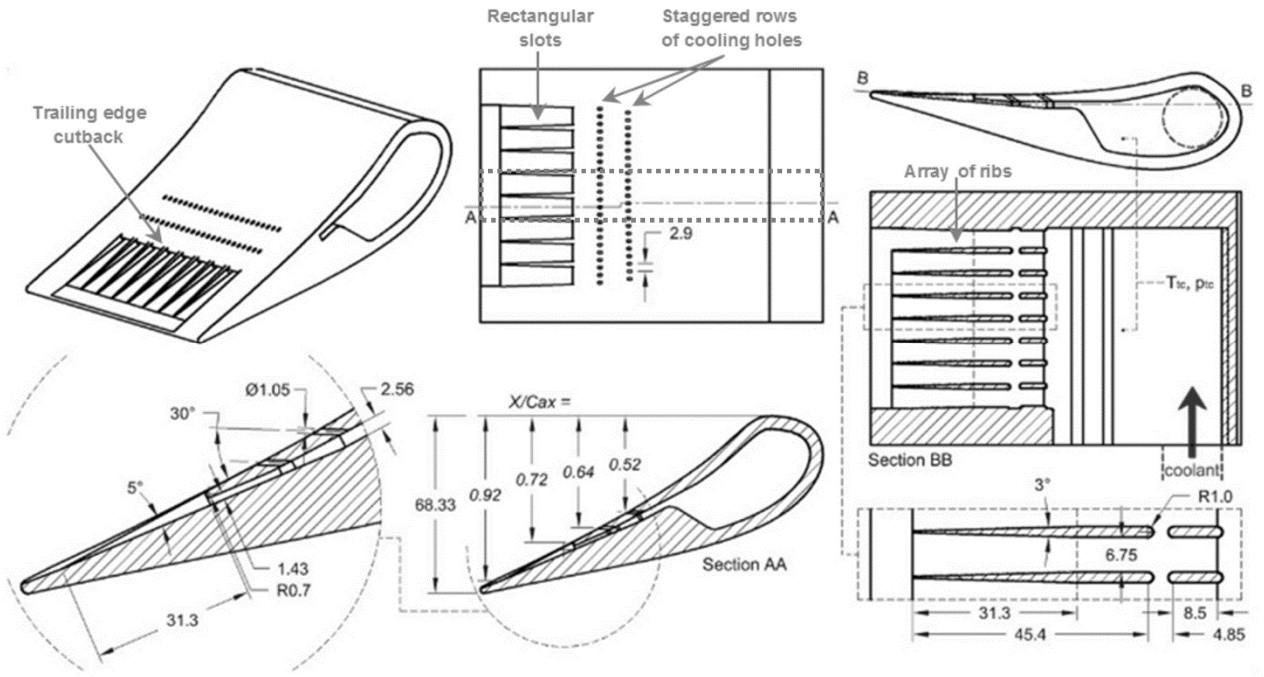

Fig. 1: Vane and trailing edge cooling geometry (size in mm) [Barigozzi et al. (2012)].

The turbulence intensity of the coolant was assumed to be 5.67% with a length scale of 1.05 mm. Air properties were set to be temperature dependent. Adiabatic conditions were applied to solid surfaces. For the injection of the coolant into the plenum, a mass flow inlet condition was specified. The coolant mass flow rate was varied to match the *MFR* of 1.44% and 2%, corresponding to MFR_{slot} of 1.14% and 1.49%.

Grid generation

All simulations were carried out on a multi-block unstructured grid (#1), then converted into a polyhedral mesh containing about 2.87 million cells (Fig. 3). The bulk of the cells was allocated in the cutback region extending from the slot exit to the trailing edge. Further local refinement in this region was implemented in grid #2: grid spacing was reduced along the x -streamwise, y - wall normal and z - spanwise directions, as indicated by $\Delta x+$, $\Delta y+$ and $\Delta z+$ values of Table 1. Accordingly, the average y+ on the cutback surface was reduced from 1.8 to 1.0. Note that averaged values of the wall shear stress were used to compute the reported $\Delta x+$, $\Delta y+$ and $\Delta z+$. Both grids were used to check grid independence for DES at *MFR* = 2%. Analysis of mesh sensitivity was based on temperature values in the cutback region. Two monitoring points (see Fig. 3) were located at midspan, close to the cutback lip (X/c_{ax} = 0.78) and approaching the trailing edge (X/c_{ax} = 0.94). Grid #1 was found to provide sufficient resolution since time averaged values of temperature at monitor points for grid #1 and #2 deviated by less than 4.5% (data were collected over 15 shedding cycles, starting from the steady solution).

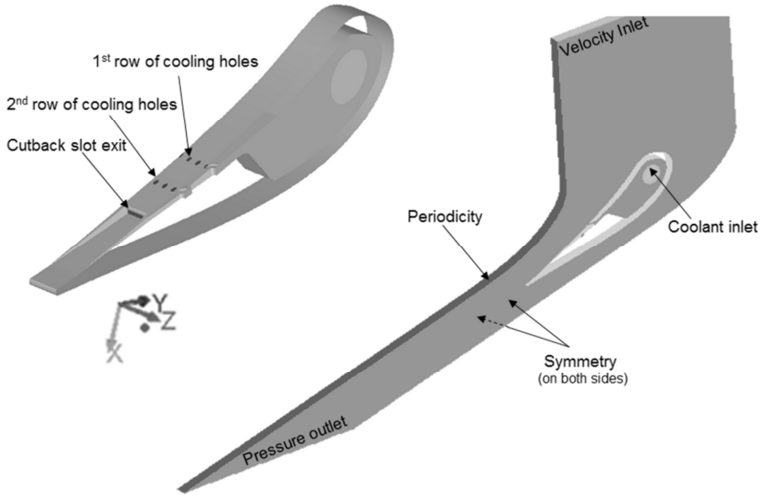

Fig. 2: 3D domain and boundary conditions.

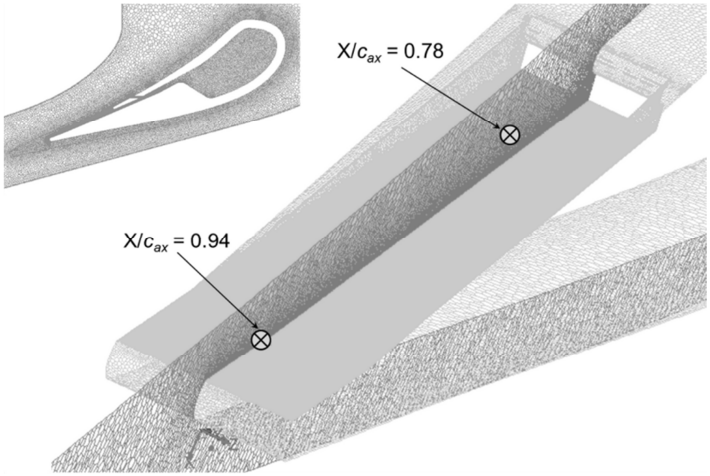

Grid	#1	#2
Tetrahedra (Million)	14.94	27.36
Polyhedra (Million)	2.87	5.12
Δx^+	6.5	3.6
Δy^+	8.6	6.8
Δz^+	1.9	1.2
Cutback averaged y^+	1.8	1.0

Table 1: Grid resolution.

Fig. 3: Grid (#1) views and details.

Numerical settings

The solutions were obtained by solving the incompressible Navier-Stokes equations. Unsteady simulations were initiated from steady simulations and advanced in time until a statistical steady state was achieved. Additional 7.6 cycles of vortex shedding (650 time steps) were computed to obtain time averaged results. The SAS model invoked a variant of the SST k-ω model which was invented by Menter and Egorov (2010). SAS works as follows: if the grid is fine enough, in the regions where the flow is on the limit of going unsteady, momentum equations resolve part of the turbulence. SAS is the safest SRS but it only works for "globally unstable" flows (Menter, 2012). A typical example of "globally unstable" flow is a flow past a bluff body. It is characterized by the formation of "new" turbulence downstream of the body which overrides the turbulence coming from the attached boundary layer around the body. DES represents a further step towards SRS. It switches between RANS and LES models based on the local grid spacing. In particular, the SST-Delayed DES (DDES) model proposed by Gritskevich et al. (2012) was chosen among the available DES shielding functions. Assuming that a fine grid is provided, DDES behaves almost like SAS for "globally unstable flow". Moreover DDES allows the SRS behavior also for "locally unstable" flows, where SAS would remain in RANS/URANS mode (Menter, 2012). In a locally unstable flow, "new" turbulence is produced downstream of a geometry change (i.e. flow past a flat plate), but the flow instability producing this turbulence is much weaker than for "globally unstable flows". The point is that the zone behind the cutback lip changes its category, from "globally unstable" to "locally unstable" flow, while increasing *MFR*. This study found that SAS does not switch to SRS mode at *MFR* = 2%, independently of mesh resolution. So DDES was required for formation of unsteadiness at the highest *MFR*. The unsteady simulations were conducted with 50 inner iterations to converge for each time step, so that residuals drop by about 4 orders of magnitude. A time step of Δt = 1.8e-6s was used for *MFR* = 1.44%. For the *MFR* of 2% case, Δt was reduced to 6.5e-7s. The Courant number in the shedding region was below unity, except in a few cells close to the trailing edge where the *CFL* was about 1.5. Time integration was carried out with the bounded second order implicit scheme. The coupled algorithm solved the momentum and the pressure-based continuity equation together. The solution control required a flow Courant number of 1. Further details about numerical settings are available in Table 2. For the sake of completeness, the *MFR* of 1.05% case (from Ravelli and Barigozzi (2014)) was reported. Both SAS and DDES were computed with steady state boundary conditions, as employed in the RANS case: unsteadiness developed due to inherent flow instability behind the cutback lip, without any forcing.

RESULTS AND DISCUSSION

Simulation results were presented to document the influence of *MFR* on vortex shedding from the cutback lip. Instantaneous contours of temperature and vorticity fields were compared with

experimental stereo PIV measurements and flow visualizations. Measurements of film cooling effectiveness on the cutback surface were also used to validate the modeling. Finally, the shedding frequency was computed from the simulations and compared with the experimental findings.

Instantaneous flow structures

In Fig. 4 instantaneous sectional views of the non-dimensional temperature θ and snapshot visualizations are placed side by side to compare the predicted and measured flow structures, in the centerline plane of the cutback region. The reader is referred to Barigozzi et al. (2012) for a full explanation of the flow visualization technique. A deeper insight into the simulated vortex shedding is provided in Fig. 5. Numerical contours of spanwise component of the instantaneous vorticity, normalized by the lip thickness and the mainstream velocity at the slot exit, are shown for the investigated *MFR*. It is advisable to point out that numerical plots at $MFR \leq 1.44\%$ contain results from SAS whereas predictions at $MFR = 2.00\%$ derive from DDES. This is because SAS had a fallback to RANS mode at the highest *MFR*, even using a proper temporal and spatial resolution (i.e. time step of 6.5e-7s and Grid#2 spacing).

Coherent periodic structures shedding from the cutback lip, due to the unsteady behavior of the shear layer between the coolant and the main flow, can be clearly seen in all simulations (Figs. 4b,d,f), with black areas being the coolant and white area the hot gas. In particular, an observer viewing the cutback as depicted in Fig. 4 can detect clockwise and counter-clockwise flow structures. For the lowest *MFR* value of 1.05%, SAS predictions showing crests of the waves clockwise in orientation (Fig. 4b) are in agreement with that indicated by experiments (Fig. 4a), at least from a qualitative point of view. Crests of the waves denote the presence of mainstream-side vortices shedding off the upper cutback lip, with negative (clockwise) vorticity. Moreover, the computed θ contours show evidence of the small vortices rolling off in a counter-clockwise manner that are observed experimentally, near the vane surface. They are coolant-side vortices with positive (counterclockwise) vorticity, as clearly shown in Fig. 5a. They are wrapped into the dominant mainstream flow vortices since the coolant velocity at the slot exit is much lower than the mainstream one at low *MFR*. An increase in the *MFR* value to 1.44% causes a radical change in the flow field. Both visualizations (Fig. 4c) and predictions (Fig. 4d) reveal the presence of coupled counter rotating vortices with a "mushroom like" shape. They are mainstream-side and coolant-side vortices shedding off in alternating pattern, since the momentum of both flows is almost of a similar magnitude. The computed vorticity plot of Fig. 5b proves that the increase in *MFR* to 1.44% causes an enhancement of the coolant side vortices (positive vorticity) both in magnitude and persistence and a weakening in the mainstream-side ones.

Case	**SAS**	**SAS**	**DDES**
MFR (%)	1.05	1.44	2.00
MFR_{slot} (%)	0.90	1.14	1.49
VR	0.73	0.91	1.20
BR	0.67	0.84	1.11
Turbulence model	SST-SAS k-ω	SST-SAS k-ω	SST k-ω
Δt (s)	2.5e-6	1.8e-6	6.5e-7
Solver	Pressure-based (incompressible flow)		
Pressure-velocity coupling	Coupled		
Spatial discretization: Momentum Energy Turbulence Gradient	 Bounded Central Differencing 2nd order upwind 2nd order upwind least square cell based		

Table 2: Numerical settings for SAS and DDES.

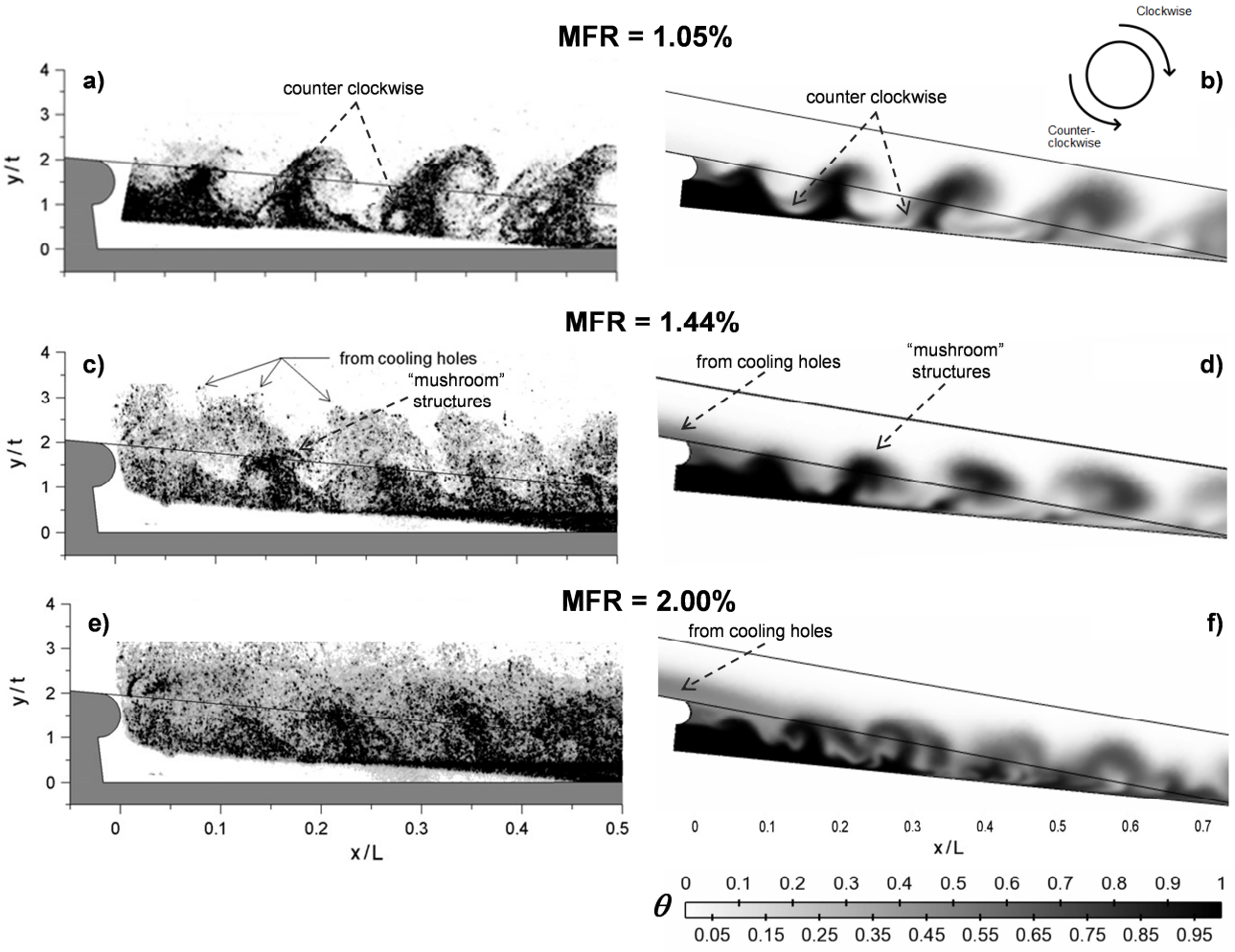

Fig. 4: Snapshots of flow visualizations (left) and instantaneous predictions (right) of the normalized temperature contours θ at midspan for a,b) *MFR* = 1.05%, c,d) *MFR* = 1.44% and e,f) *MFR* = 2.00%.

When *MFR* is further increased to 2.00%, DDES results (Fig. 4f) indicate that wave-forms appear again but oriented in the reverse directions. This is in agreement with flow visualization in Fig. 4e, showing periodical dark regions of high coolant concentrations with an oblique, backward structure. At the highest *MFR*, the velocity of the coolant exiting the slot and flowing over the cutback surface is high enough to further reinforce the coolant-side vortices with counterclockwise rotation, with respect to the case at *MFR* =1.44%. As a consequence the mainstream-side vortices can be hardly seen, as shown in Fig. 5c.

Additional similarities between flow visualizations and numerical θ contours relate to the behavior of the coolant exiting from the cooling holes located upstream of the cutback slot. In fact the simulations at *MFR* > 1 (Figs. 4d,f) confirm that a significant amount of coolant ejected from the upstream cooling holes mixes with the coolant issued from the slot, thus reducing the clearness of the contour plots in the cutback region. As a final point, vortex evolution depicted in Fig. 5 proves that SAS (Figs 5a,b) and especially DDES (Fig. 5c) produce both large-scale unsteadiness (primary instability) and streamwise small scale vortices (secondary instability), with the latter persisting up to the trailing edge.

Thermal mixing process

The spatial distributions of adiabatic effectiveness predicted with unsteady simulations and measured experimentally are compared in Fig. 6, for different injection conditions. SAS and DDES instantaneous and time averaged effectiveness contours are provided for each *MFR*. Measured plots

of adiabatic effectiveness (by means of Thermochromic Liquid Crystals) are also shown for validation at *MFR* of 1.05% and 2.00%. The uncertainty in the measured film cooling effectiveness depends on TLC and thermocouple measurements and on conduction effects. In the regions where conduction effects are negligible, η uncertainty ranges from ± 4.2% with η = 0.8, up to ±15% when η = 0.1. For further details on thermal measurements, the reader is referred to Barigozzi et al. (2012a). The instantaneous results were reported to document how unsteadiness affects the thermal coverage on the cutback surface. At a first glance, adiabatic effectiveness values at increasing distance from the slot exit are quite similar for time averaged predictions and experiments, whatever the *MFR*. This is of extreme importance: SAS and DDES succeeded where steady RANS and URANS failed. As far as the lateral spreading is concerned, both SAS and DDES predicted a laterally less uniform adiabatic effectiveness than measured data, approaching the trailing edge.

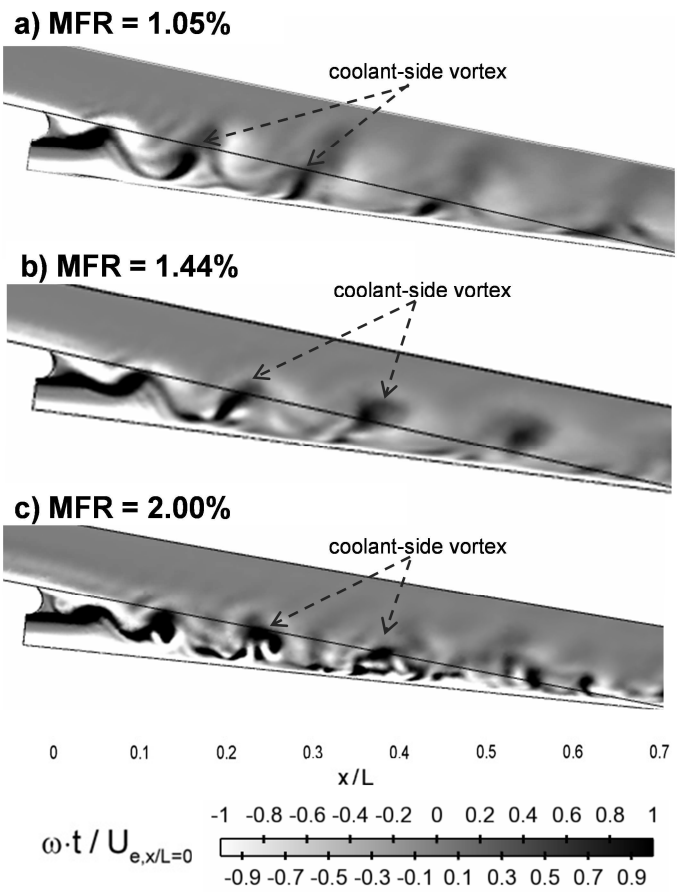

Fig. 5: Predictions of the normalized spanwise vorticity at midspan at *MFR* = 1.05% (a), 1.44% (b) and 2.00% (c).

At the lowest *MFR*, SAS computed a streamwise extension of the core region (where η reaches the maximum level) similar to that measured. Downstream of the core region, the coolant stream is broken up. As described in the previous section, the mainstream-side vortices, with clockwise vorticity, transport hot gas close to the wall and coolant flow away from the wall, thus lowering film cooling efficiency. The resulting decay of thermal protection along the cutback surface is well predicted by SAS. The numerical η levels at the trailing edge are as low as 0.2, in agreement with TLC measurements. Increasing the *MFR* to 1.44%, the coolant flows a little further along the cutback surface so higher values of η can be found at a higher distance from the slot exit, as compared to the case at the lowest *MFR*. The core region is less marked as well as streamwise temperature gradients over the cutback surface. This is due to the strengthened coolant-side vortices evolving near the vane. They obstruct the transport of heat towards the wall by the mainstream-side vortices. Consequently, a slight improvement in cooling efficiency is predicted when increasing *MFR* from 1.05% to 1.44%, even at the trailing edge. A further increase in *MFR* to 2.00% leads to an additional enhancement of both the computed and the measured thermal coverage distributions. At the highest *MFR*, deterioration of film cooling effectiveness along the cutback becomes less severe thanks to the dominant coolant-side vortical structures. However, the trailing edge cooling is not as effective as expected since experiments indicated $\eta < 0.3$ at the trailing edge. DDES was not able to predict such a poor cooling efficiency on the rear cutback: some overestimation of film cooling effectiveness, especially at the end of the vane, is still present when comparing Fig. 4g with Fig. 4h.

For a quantitative comparison between numerical predictions and experimental data, the cooling effectiveness on the cutback surface was laterally averaged over the span (Fig. 7). Data are plotted against the normalized distance between the slot exit and the end of the vane (x/L_c is shown in Fig. 6). Time averaged SAS and DDES results are verified against measurements at *MFR* = 1.05% and

2.00%. Steady RANS predictions are also included for reference. SAS predictions of η_{av} at *MFR* = 1.44% were not reported in Fig. 7 since there are no experimental data to compare with. A detailed discussion of the discrepancies between measured and predicted η_{av} values in the cutback region within $0 < x/L_c < 0.2$ can be found in Ravelli and Barigozzi (2014). Here attention has been drawn to the region at $x/L_c > 0.2$, i.e. where the simulated coolant stream is broken up and η_{av} starts decreasing. No correction was applied to exclude ribs when computing η_{av}. According to the simulations, the rib surface is hotter than the cutback one. This is why the peak η_{av} values in the RANS simulations resulted at about half of the cutback length. Conversely, experiments showed that the rib surface is colder than the cutback one, due to imperfect adiabatic conditions.

At *MFR* of 1.05%, SAS satisfactorily predicts the measured levels of η_{av} for $x/L_C > 0.2$. In more detail, η_{av} is slightly underpredicted by SAS in the region within $0.35 < x/L_C < 0.8$. A reason for this can be found considering the contribution of ribs to η_{av}. In fact, ribs are colder in the experiments than in the simulations. On the opposite, η_{av} values by SAS are a little higher than measured experimentally in the region close to the trailing edge, for $x/L_C > 0.8$. At the trailing edge SAS yields $\eta_{av} = 0.18$ compared to the experimental value of $\eta_{av} = 0.11$. At *MFR* = 2.00%, DDES is much better than RANS, but overestimation of η_{av} is still present on the whole cutback. However, DDES correctly simulates the trend in $\eta_{av,}$ showing an almost linear film degradation while progressing downstream along the cutback. Unfortunately, the largest difference between modelled and experimental η_{av} values can be detected at the trailing edge (DDES yields $\eta_{av} = 0.54$ compared to the experimental value of $\eta_{av} = 0.26$), since DDES does not predict the abrupt decrease in η_{av} which is measured at $x/L_C > 0.9$.

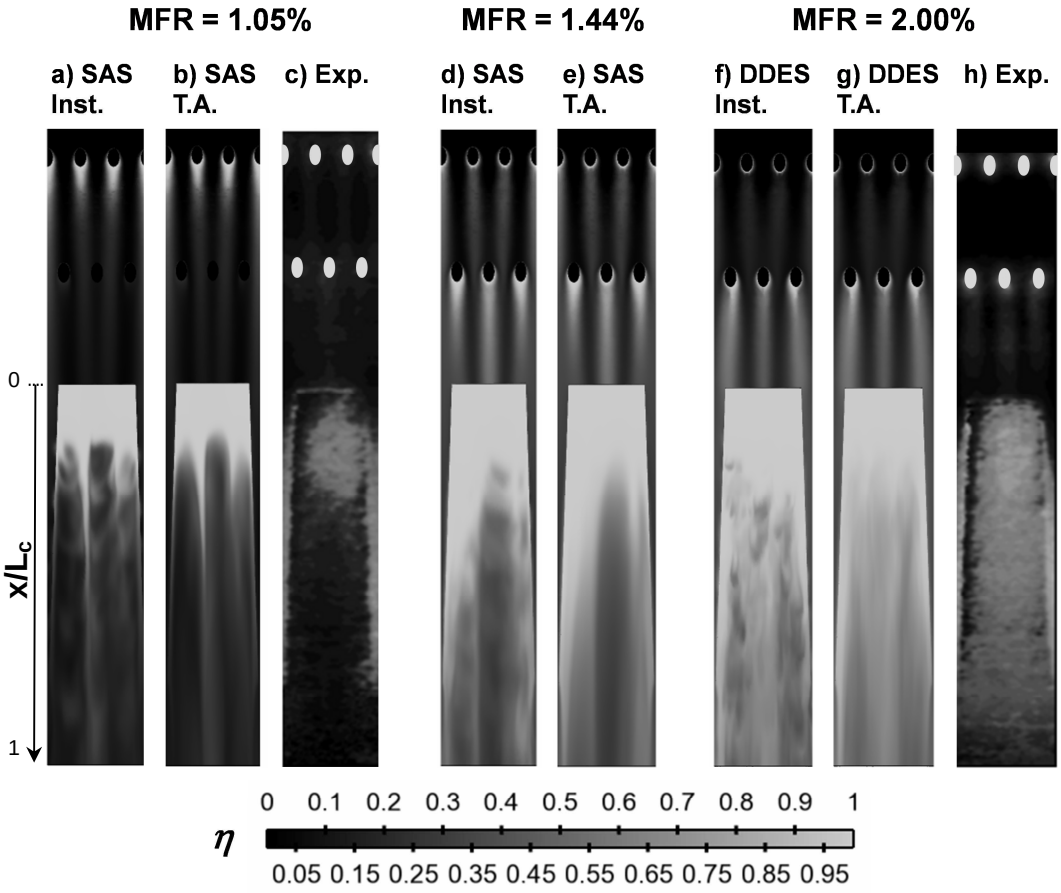

Fig. 6: Experimental measurements (Exp.), Instantaneous (Inst.) and time averaged (T.A.) SAS and DDES predictions of the adiabatic effectiveness η at *MFR* = 1.05% (a-c), 1.44% (d, e) and 2.00% (f-h).

Actually, an increase in *MFR* resulted in a more significant overprediction of η_{av} at the trailing edge. Weakening of vortices and thermal mixing at increasing distance from the slot exit, due to numerical dissipation, may be aggravated by high *MFR*. Recent works pointed out that the dissipation level of the numerical scheme is very important, even when coupling with advanced DDES (Xiao et al. (2012)). What is more, it should be clarified that simulations and experiments having the same *MFR* may result in slightly different MFR_{slot} values, depending on the coolant flow sharing between cutback and cooling holes. The gap between the measured and the computed MFR_{slot} values is larger at higher *MFR*. In particular, simulations at *MFR* of 2.00% tend to overpredict MFR_{slot}, i.e the amount of coolant exiting the cutback slot, at the expense of that discharged through the cooling holes. This may partially explain why the predicted η_{av} at *MFR* = 2.00% is higher than the measured one over the whole cutback.

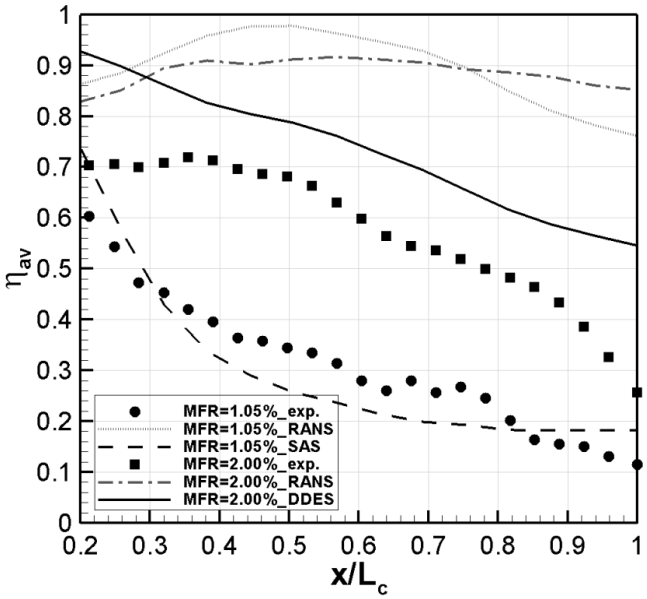

Fig. 7: Measurements (exp.) and predictions of the laterally averaged adiabatic effectiveness η_{av} over the cutback surface, at *MFR* = 1.05% and 2.00%.

Shedding frequencies

Finally, the Strouhal number *St* was computed using the average magnitudes of both the mainstream and coolant velocity at the slot exit as the velocity scale. The lip thickness was used as the length scale and the frequency was taken from the FFT analysis of the time varying velocity components and spanwise vorticity at both selected monitor points (Fig. 3). Simulations delivered *St* number of 0.27, 0.25 and 0.31, for *MFR* = 1.05%, 1.44% and 2.00%, respectively, to be compared with the corresponding measured *St* values of 0.43, 0.40 and 0.48. Computations underpredict the shedding frequency whatever the *MFR*. At least they capture the trend in *St* showing a minimum *St* for the intermediate *MFR*, i.e. when both mainstream-side and coolant-side vortices shed off in alternating pattern from the lip.

CONCLUSIONS

Predictions of vortex shedding and thermal mixing from SAS and DDES modelling of trailing edge cutback film cooling were validated against measurements performed in a nozzle vane cascade, at low velocity. Different *MFR* values were considered in a range allowed to develop natural flow unsteadiness (1.05% ≤ *MFR* ≤ 2.00%). The changes in the mainstream-side and coolant-side vortices behind the lip as *MFR* increases were well predicted by the SRS simulations. As far as the cutback thermal coverage is concerned, results from simulations (averaged in time and spanwise direction) and experiments showed a comparable degradation of the film cooling effectiveness with increasing distance from the slot exit. Nevertheless, some overestimation of the numerical η was found at the trailing edge, especially for the highest *MFR*. Neither SAS nor DDES succeeded in predicting a shedding frequency as high as measured, whatever the *MFR*.

In addition, it was shown that the flow behind the cutback lip, which is considered "globally unstable" in the published literature, has the features of a "locally unstable" flow if a large coolant flow rate exits the cutback slot. Accordingly, at the highest investigated *MFR*, DES was the only hybrid method to develop inherent unsteadiness behind the cutback lip. SAS was found to be suitable for modeling vortex shedding and thermal coverage over the cutback surface at *MFR* ≤ 1.44.

ACKNOWLEDGEMENTS

The authors gratefully acknowledge the Italian Ministry of Instruction, University and Research (MIUR) for funding this research project (PRIN2010-2011). Moreover, this work has been supported by Regione Lombardia and CINECA Consortium through a LISA Initiative (Laboratory for Interdisciplinary Advanced Simulation) 2012-2014 grant. Special thanks to the colleagues from the University of Udine for performing PIV measurements. Finally, Prof. Perdichizzi is gratefully acknowledged for his support.

REFERENCES

Barigozzi G., Armellini A., Mucignat C., Casarsa L., (2012), *Experimental Investigation of the Effects of Blowing Conditions and Mach Number on the Unsteady Behavior of Coolant Ejection through a Trailing Edge Cutback*, Int. J. Heat Fluid Fl. 37, 37-50.

Barigozzi G., Perdichizzi A., Ravelli S., (2012a), *Pressure Side and Cutback Trailing Edge Film Cooling in a Linear Nozzle Vane Cascade at Different Mach Numbers*, J. Turbomach. 134(5), 051037-1:10.

Egorov Y., Menter F. R., Lechner R., Cokljat D., (2010), *The Scale-Adaptive Simulation Method for Unsteady Turbulent Flow Predictions. Part 2: Application to Complex Flows*, Flow Turbulence Combust. 85, 139-165.

Gritskevich M. S., Garbaruk A.V., Schutze J., Menter F. R., (2012), *Development of DDES and IDDES Formulations for the k-ω Shear Stress Transport Model*, Flow Turbulence Combust. 88, 431-439.

Joo J., Durbin P., (2009), *Simulation of Turbine Blade Trailing Edge Cooling*, J. Fluids Eng. 131(2), 021102-1:14.

Krueckels J., Gritsch M., Schnieder M., (2009), *Design Considerations and Validation of Trailing Edge Pressure Side Bleed Cooling*, ASME Paper GT2009-59161, 63-70.

Martini P., Schulz A., Bauer H. J., Whitney C. F., (2005), *Detached Eddy Simulation of Film Cooling Performance on the Trailing Edge Cut-back of Gas Turbine Airfoils*, J. Turbomach. 128(2), 292-299.

Martini P., Schulz A., Whitney C. F., Lutum E., (2003), *Experimental and Numerical Investigation of Trailing Edge Film Cooling downstream of a Slot with Internal Rib Arrays*, Proc. 5th European Conference on Turbomachinery Fluid Dynamics and Thermodynamics, 487-500.

Menter F. R., (2012), *Best Practice: Scale-Resolving Simulations in ANSYS CFD*, Version 1.0, ANSYS Report.

Menter F. R., Egorov Y., (2010), *The Scale-Adaptive Simulation Method for Unsteady Turbulent Flow Predictions. Part I: Theory and Model Description*. Flow Turbulence Combust. 85, 113-138.

Ravelli S., Barigozzi G., (2013), *Evaluation of RANS Predictions on a Linear Nozzle Vane Cascade with Trailing edge Cutback Film Cooling*, ASME Paper GT2013-94694, pp. V03BT13A030; 12 pages.

Ravelli S., Barigozzi G., (2014), *Application of Unsteady CFD Methods to Trailing edge Cutback Film Cooling*, J. Turbomach. 136(12), 121006-121006-11.

Ravelli S., Miranda M., Barigozzi G., (2013), *Steady CFD Simulations of Trailing Edge Film Cooling in a Linear Nozzle Vane Cascade*, Proc. 10th European Turbomachinery Conference, Lappeenranta, Finland.

Schneider H., von Terzi D., Bauer H.-J., (2010), *Large-Eddy Simulations of Trailing-edge Cutback Film Cooling at Low Blowing Ratio*, Int J Heat Fluid Fl. 31, 767-775.

Schneider H., von Terzi D., Bauer H.-J., (2012), *Turbulent Heat Transfer and Coherent Structures in Trailing-edge Cutback Film Cooling*, Flow Turbulence Combust. 88, 101-120.

Xiao Z. X., Liu J., Huang J.B., Fu S., (2012), *Numerical Dissipation Effect on the Massive Separation around Tandem Cylinders*, AIAA J, 50 (5), 1119–1136.